THE ASTRONOMICAL JOURNAL, 116:1992–1997, 1998 October

10 MICRON SEARCH FOR COOL COMPANIONS OF NEARBY STARS

DAVE VAN BUREN AND MICHAEL BRUNDAGE
Infrared Processing and Analysis Center, Mail Stop 100-22, California Institute of Technology, Pasadena, CA 91125
MICHAEL RESSLER
Jet Propulsion Laboratory, California Institute of Technology, 4800 Oak Grove Drive, Pasadena, CA 91109
AND
SUSAN TEREBEY
Extrasolar Research Corporation, 720 Magnolia Avenue, Pasadena, CA 91106
Received 1997 November 7

ABSTRACT

We present 10 μm broadband images of the nearby stars Gliese 15, 71, 628, 699, 725A, 725B, 729, and 820A from an experiment designed to detect cool companions. The observations establish upper limits for the presence of companion objects with separations between 2″ and 10″ at or below the hydrogen burning limit for Gliese 15, 699, and 729.

Key words: planetary systems — stars: low-mass, brown dwarfs — techniques: image processing

1. INTRODUCTION

With the discovery of Gliese 229B (Nakajima et al. 1995), the low-mass companion to Gliese 229, it is now clear that substellar objects in the mass range 1 decade below the hydrogen burning limit exist in at least moderate numbers. In anticipation of a dynamical mass for Gliese 229B under 0.08 $M_{\odot}$, attention now turns toward determining the frequency, taxonomy, formation, evolution, and astrophysical consequences of brown dwarfs and massive extrasolar planets.

In carrying out this program, it is essential to obtain a sizable sample of objects that can be studied in detail. A number of approaches have been proposed and are being pursued, including astrometric and velocity monitoring, coronagraphic imaging, and mid-infrared imaging of nearby stars from the ground and space. Because this is an empirical problem, a broad suite of search strategies is important. In this short paper, we describe exploratory 10 μm imaging of nearby stars from the Palomar 5 m telescope. This wavelength is appropriate for a search because the blackbody peaks for companions with temperatures between 100 and 1000 K are near this wavelength. Our experiment is formally capable of detecting objects with a flux density greater than 10 mJy in the separation range 2″–10″ from the primary. While the flux limit is much shallower than can be achieved from space (e.g., with the *Infrared Space Observatory*), it probes a separation range not accessible to orbital telescopes by using the small diffraction-limited beam available to a large telescope.

Current successful methods for detecting massive extrasolar planets, i.e., radial velocity and astrometric methods, are primarily sensitive to short periods and, hence, small orbits of order 3 AU or less. The direct detection experiment explored here is of considerable interest because it is sensitive to planets in 3–50 AU orbits about their primaries, in the range where gas giant planets are predicted to form (Pollack et al. 1996; Boss 1995).

Models for planet formation, developed to explain our own solar system, have planets forming via the accumulation of solid particles (dust and ices) from the size of grains to planetesimals. When rocky cores reach 10–20 Earth masses, the nebular gas can accrete, forming gas giants (Pollack 1984). Given this picture, the surprising discovery of massive planets at sub-AU distances from their primaries has led to a view in which planets undergo inward orbital migration from their birthplaces outside the ice condensation radius of 3–5 AU (Trilling et al. 1998).

A direct 10 μm search for cool companions and massive extrasolar planets is a reasonable experiment in terms of the yield per target, based on the following statistics:

1. Six percent of solar-type stars have giant planets, $m \sin i > 0.5\ M_{\rm Jup}$, within 3 AU (Marcy & Butler 1998). Interestingly, this cutoff would exclude our solar system.
2. Two percent have brown dwarfs within 5 AU (Mayor 1998).
3. There is a roughly 10% incidence rate of stellar companions for each decade in orbital size (Fischer & Marcy 1992). If the incidence rate of companions is nearly mass independent (which seems plausible given the first point above), then there are a correspondingly large number of brown dwarf and giant planets.

Ultimately, several tens of stars must be observed with sufficient sensitivity to begin addressing the issues raised above. This class of experiments, 10 μm direct imaging, has the potential to quickly reach that goal.

2. OBSERVATIONS

We carried out our observations during the nights of 1996 August 14 and 15 (UT) with the MIRLIN camera (Ressler et al. 1994) at the Cassegrain focus of the 5 m Hale Telescope at Palomar Observatory. MIRLIN uses a 128×128 array detector with a 20″ field of view. The instrument manual quotes a sensitivity of $\approx$10 mJy hr$^{-1/2}$ at the broadband N filter (10.2 μm) in which we observed. The weather during the observations was nonphotometric, and data taking was interrupted at one point by light precipitation.

We observed eight targets, spending on average 1 hr on each. We chopped and nodded to remove first- and second-order sky-induced drifts. Usually the chopper throw and nod offset were 8″ (on-chip chopping and nodding), although some data were taken with larger throws and offsets to eliminate any source aliasing. Because on-chip

TABLE 1

JOURNAL OF OBSERVATIONS

Star	Start Time (1997 UT)	Chop/Nod Sets	Spacing (arcsec)	Integration Time (s)
Gliese 15	Aug 14 1054	19	8, 10	2228
Gliese 71	Aug 15 1131	2	8	240
Gliese 628.....	Aug 14 0358	17	8	2040
Gliese 699.....	Aug 15 0318	21	8	2520
Gliese 725A.....	Aug 14 0600	9	8	1080
Gliese 725B.....	Aug 14 0634	8	8	960
Gliese 729.....	Aug 15 0507	18	8	2160
Gliese 820A.....	Aug 15 0719	14	8	1680

chopping and nodding eliminates off-target data at the slight loss of a small fraction of the sensitive field of view, we favor it for experiments aimed at small separations. Over the course of the observing a single object, we dithered the pointing center by a few arcseconds to suppress detector artifacts. Table 1 is a journal of our observations indicating our targets, starting times, number of chop-nod cycles, and chop-nod offsets.

The instrument data system produces flat FITS files containing co-adds at each chopper position and ancillary metadata typical of any camera experiment. The data were reduced using a collection of IDL functions implementing a lightweight reduction system in about 500 lines of code.

A single observation cycle is made up of four images: two chopper co-adds at two nod positions. Let the first index be the nod position and the second be the chopper position; then these four images can be called $I_{jk} = I_{11}, I_{12}, I_{21}, I_{22}$, with I_{11} and I_{12} being the chopped pair at the first nod position. The reduction starts by constructing a mask, M_{jk}, corresponding to each image that flags bad pixels. There are two classes of bad pixel: there is a fixed pattern where one of every 16 pixels produces bad data because of a problem in the electronics; the second class is composed of temporarily noisy or hot pixels determined from the data themselves. If a pixel is too many standard deviations different from its neighbor, it is masked out. Because the point-spread function is heavily oversampled, masked pixels are replaced with the median of their neighbors to cosmetically repair the data. The repaired images, $R(I_{jk})$, are then flat-fielded using a median flat generated from the four input frames to give the flattened images $F(R(I_{jk}))$. Next, we compress the images by a factor of 4 in each dimension by summing 4×4 groups of pixels and constructing a mask containing the corresponding 4×4–summed mask values. The resulting images, $C(F(R(I_{jk})))$, are slightly undersampled with respect to the Nyquist frequency of the telescope beam and are close to optimizing the signal-to-noise ratio per pixel for point-source detection.

The next step in the processing constructs the difference images $C_{11} - C_{12}$ and $C_{21} - C_{22}$. These difference images are themselves differenced to give $Q(C(F(R(I)))) = C_{11} - C_{12} - C_{21} + C_{22}$, which removes the sky and its first-order spatial derivatives. Q and $-Q$ are now shifted and co-added, so each appearance of the primary is placed at the center of the resultant map, yielding an image $S(Q(C(F(R(I)))))$, where the primary is aliased eight times. Any real source inside the chop-and-nod bounding box will likewise be aliased up to eight times. This procedure is cycled through for all sets of quadruples I_{jk} comprising the set of observations for a single target. In one case both stars

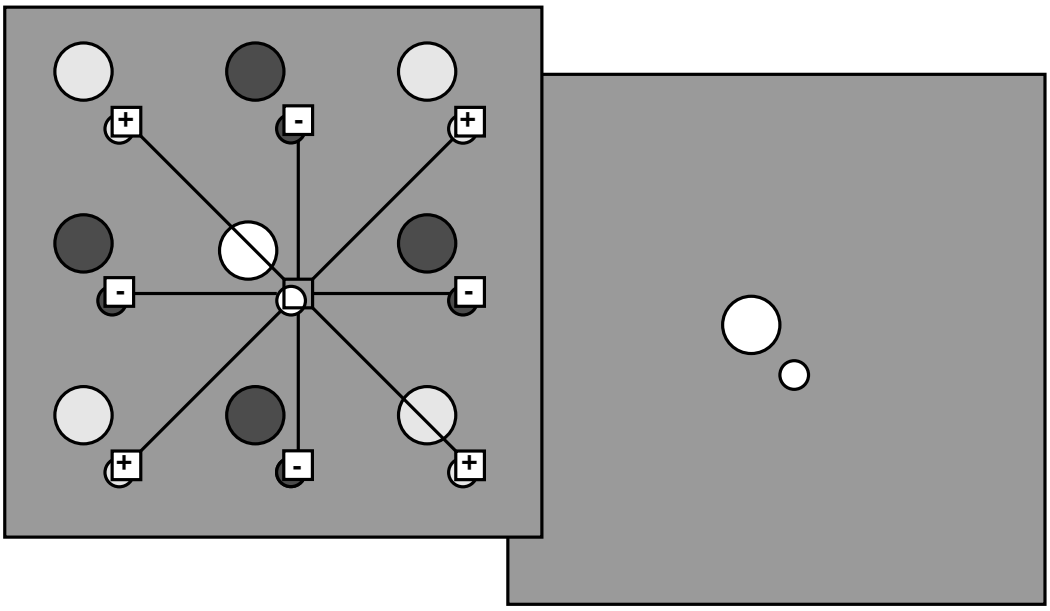

FIG. 1.—The logical filtering operation. An eight-point filter is passed over the image (*left*), whose output (*right*) is zero if the deviations from the mean background are not all in the same direction as that expected for a source aliased to the eight points in the co-add. Otherwise, the output is the pixel value at zero lag. This filter suppresses source aliases.

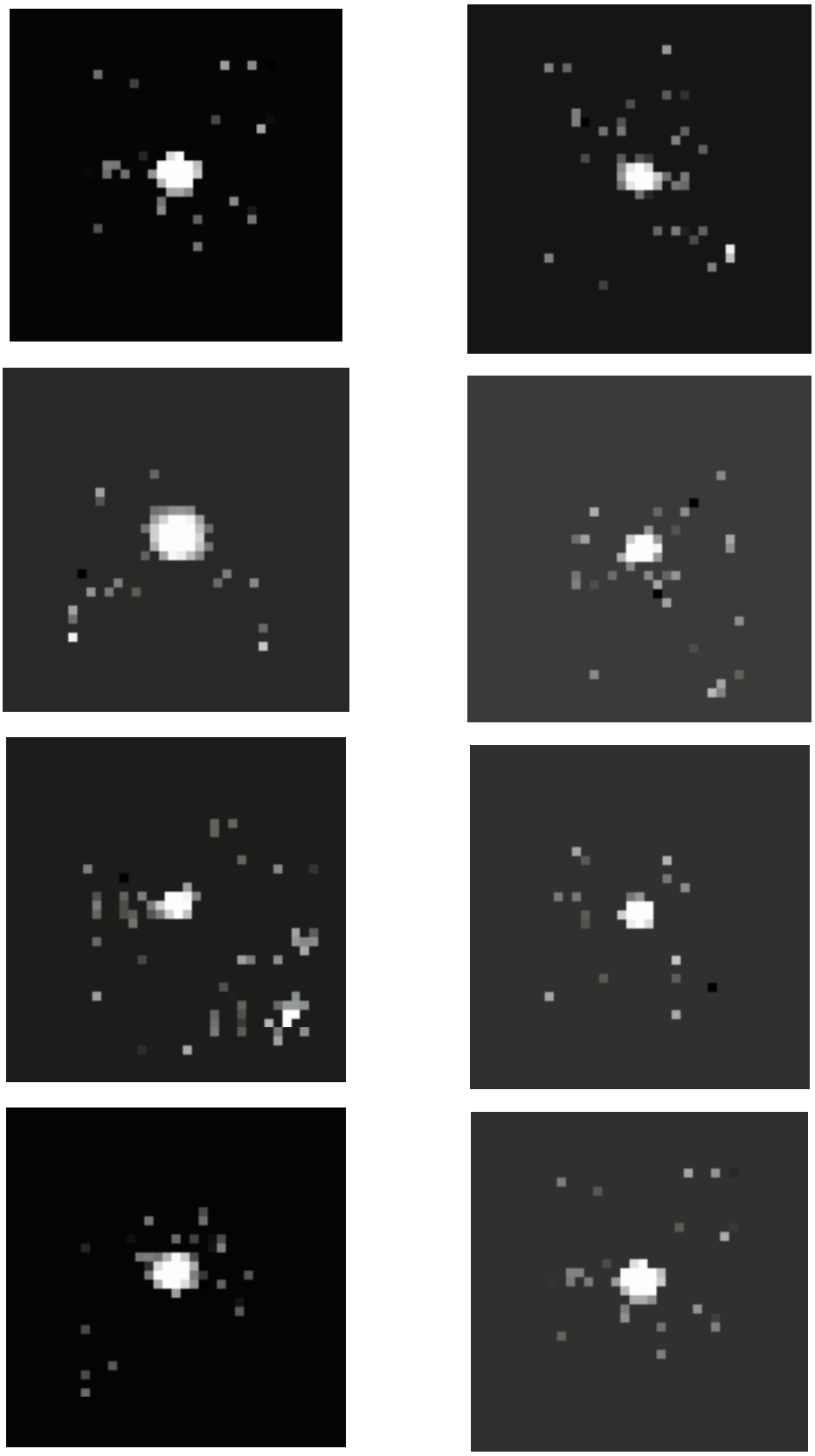

FIG. 2.—Logically filtered on-chip chop-and-nod co-adds of the eight target stars made with MIRLIN. *Top to bottom, left to right*: Gliese 15, 71, 628, 699, 725A, 725B, 729, 820A. Each image is about 10″ on a side. We set the detection upper limits to be the magnitude of the strongest off-primary nonaliased pixel with a neighboring nonzero pixel. A strong alias of the primary is present in the lower right corner of the Gliese 628 filtered image. Likewise, the apparently significant object at 4 o'clock in the Gliese 725A image is an alias of Gliese 725B, which appears in the southern nod frames of the Gliese 725A observations.

TABLE 2

OBSERVATIONAL RESULTS

Star	N-Band Flux Density (Jy)	1 σ Noise (mJy)	Upper Limit (mJy)
Gliese 15	4.5	10	40
Gliese 71	23.7	211	670
Gliese 628.....	2.0	43	165
Gliese 699.....	2.8	23	57
Gliese 725A.....	3.9	60	161
Gliese 725B.....	2.4	74	181
Gliese 729.....	1.4	48	78
Gliese 820A.....	17.0	36	125

of a known binary were targeted. The two fields were treated separately rather than being mosaicked together.

Images obtained after this reduction contain aliased sources, confusing the identification of any faint objects that may be present. A more straightforwardly interpreted image of the field is finally made by taking into account the aliasing pattern. To construct this final image, we perform a logical filtering operation $\mathscr{L}(Q)$ on the image, passing pixel values unchanged when the signal at aliased positions deviates from the background in the proper direction for a real source, and setting all other pixels equal to zero. An image containing random noise treated in this fashion will pass a fraction 2^{-8} pixels, or 0.4%.

We expect that by chance there will be a few pixels passed in the field away from the image of the primary, which would lead to an impermissively high false-detection rate. This rate is dramatically lowered by taking advantage of the fact that a real source appears in several neighboring pixels because of the spatial sampling. In the absence of systematics, a block of four adjacent pixels in the final image virtually guarantees that a source was detected at that position. Unfortunately, aliases of bright sources, as well as uncalibrated instrumental and background drifts, significantly reduce the significance of passed pixels to the point where each potential source must be investigated in further detail. In Figure 1, we show schematically how the logical filter operates on an input co-add containing sources and their aliases to produce the ouput image in which the aliases are suppressed.

In setting our upper limits for detections, we use the fluxes corresponding to the brightest pixels passing the logical filter that have at least one neighbor and are not confused with aliased images of the primary. Since there are usually a few such pixels and we expect, a priori, that low-luminosity companions are not too common at our sensitivity level, it is justified to use these noise excursions to set upper limits.

3. RESULTS

For each target, we generate logically filtered co-adds using the procedure just described. These are reproduced in Figure 2. In these images, nonzero pixels formally have statistically significant positive flux, and groups of adjacent pixels would correspond to real sources in the absence of systematics. Often, candidate sources are aliased known sources; for example, the image of Gliese 725A contains an aliased image of Gliese 725B that was passed by the logical filter, an event that has unremarkable probability. Another source of systematic error is introduced primarily by the atmosphere. Rapidly changing conditions can result in uncalibrated large-scale structure in the flat fields, which locally biases the zero point, leading to an amplification of the noise peaks.

A real source at the projected position of an alias will suffer strong confusion. The immediate neighborhoods of aliases are thus, to first order, not sampled at all. Filling in these areas would require taking data with different chopper and nod offsets to move the sky positions of aliases around. We did obtain a small amount of data in this mode, and we will improve future experiments by splitting the time on each target into two sets, each with different sampling geometry.

Table 2 summarizes the observational results. For each target, we note its name; its estimated N-band flux density either based on its *IRAS* 12 μm flux density or, for the case of Gliese 725B, calibrated against a companion whose 12 μm flux density is known; the measured rms noise in the co-added (but not logically filtered) image; and the detection limit based on the brightest noise pixel that also has a neighbor present in the image passing the logical filter. All primaries are well detected. No new objects are present at the 95% confidence level. Unfortunately, the depth of coverage is not uniform, because atmospheric conditions during the observations caused the transparency to vary by a factor of 3 and the background to vary by a factor of 15.

4. DISCUSSION

The goal of our search was to apply mid-infrared imaging techniques to the problem of detecting substellar companions to nearby stars. This modest goal was met in spite of weather conditions preventing us from achieving high sensitivity. Nonetheless, our data place some constraints on the presence of substellar companions of the target stars.

Ground-based 10 μm searches for faint companions are competitive with space experiments at close separations, inside a few times the diffraction beam of the space experiments (i.e., within 10″–15″). At greater separations, the far lower backgrounds achievable with a space experiment yield sensitivities of a few mJy or less. Reaching 10 mJy limits within 10″–15″ of stars from the ground requires large telescopes and hours of integration time per target.

These fiducials define the parameter space of the experiment. At a distance of 5 pc, 10″ is 50 AU, and orbital periods for companions at these semimajor axes are millenia for K and M star primaries. A 10 mJy substellar object with a radius 0.1 $R_\odot$ has a brightness temperature of 1160 K when at 5 pc. This sensitivity is achievable in good weather with MIRLIN in about 1 hr of telescope time. Our experiment does set interesting upper limits to the brightness temperature of any low-mass companions in the surveyed range of projected separations for three of the targets.

In interpreting our results, we use the brown dwarf cooling curves computed by Nelson, Rappaport, & Joss (1993, hereafter NRJ). Table 3 transforms the observational results into useful physical parameters in the context of brown dwarfs and low-mass companions to stars: the range of projected separations sampled by the experiment on each star; the brightness temperature upper limit obtained from the flux upper limit following the assumption of a pure blackbody spectrum and taking a source size of 0.1 $R_\odot$; and, last, the corresponding mass upper limit for nonstellar objects using the evolutionary tracks in the ($T_{\rm eff}$, age)-plane. In setting these upper limit bars, we use age indicators from

TABLE 3

BRIGHTNESS TEMPERATURE AND MASS LIMITS FOR LOW-MASS COMPANIONS

Star	Projected Separation (AU)	Brightness Temperature Upper Limit (K)	Mass Upper Limit ($M_\odot$)
Gliese 15.....	9–36	1800	0.083–0.084
Gliese 71.....	9–37	22000	...
Gliese 628.....	9–43	7400	...
Gliese 699.....	4–18	1000	0.070–0.080
Gliese 725A.....	7–35	5400	...
Gliese 725B.....	7–35	6300	...
Gliese 729.....	6–30	2300	0.045–0.086
Gliese 820A.....	7–35	4300	...

Leggett's (1992) compilation, translated as "young," older than 10^8 yr; "old," older than 5×10^{10} yr and forcing $T_{\rm eff} = T_{\rm brightness}$, which could be in error by a factor of order unity. The smallest upper limit we set was 0.045 $M_\odot$ for Gliese 729. Figure 3 shows the NRJ cooling curves with our three interesting nondetections overlaid.

Our sample of three objects within the region of applicability for the brown dwarf cooling function is not sufficiently large to make any significant global statistical statements. Instead, they show that this class of experiment begins to probe an interesting region of parameter space. A heuristic rule for obtaining the fraction of stars that have binary companions in a given decade of projected separations is that roughly 10% do (see, e.g., Fischer & Marcy 1992). If this heuristic persists into the substellar mass regime, then we expect about 7% of the surveyed stars to have companions in the sampled separation range with any mass less

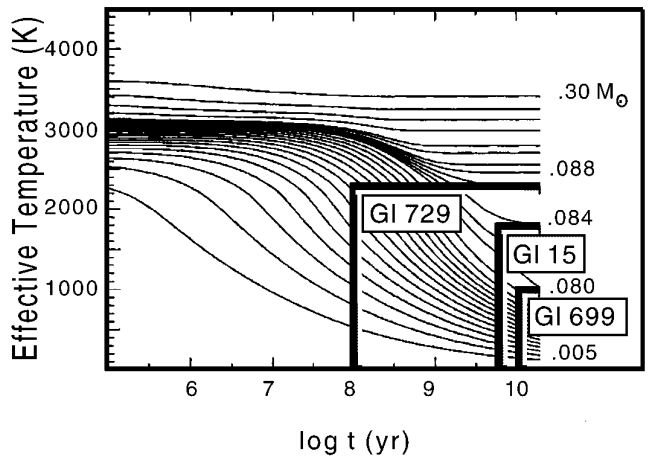

FIG. 3.—Allowed regions for companion masses plotted with the NRJ brown dwarf cooling curves on the ($T_{\rm eff}$, age)-plane. The tops of the allowed regions correspond to the upper limit flux values, and their left ends are determined by adopting lower age limits of 10^8, 5×10^9, and 10^{10} yr for Gliese 729, 15, and 699, respectively. All the other stars have effective temperature upper limits in the range 4200 to 22,000 K (for radii of 0.1 $R_\odot$), which would imply stellar (not substellar) masses of any detections. This figure was adapted from one appearing in NRJ with the kind permission of the authors.

than the primary's. Our experiment is too small to begin to measure the abundance of substellar companions by a factor of 10 or so; it is even too small to rule out the possibility that 80% of all nearby stars have substellar companions in the sample range of projected separations and brightness temperatures at the 99% confidence level.

This kind of experiment is clearly feasible and, if improved, has the potential to advance the state of knowledge regarding low-mass companions to stars. There are a number of directions to go in improving the experiment:

1. More targets;
2. Improved targets;
3. Larger sampled range of projected separations;
4. Higher sensitivity.

Extending to more targets, eventually the target list includes the entire set of nearby stars with more distant stars so far away that their companions become very difficult to detect because of their faintness. Improving the target list by choosing young stars biases the sample toward objects whose low-mass companions are on the high-luminosity lefthand side of the brown dwarf cooling curve and, hence, brighter and easier to detect. Going to a larger sampled range of projected separations increases the detection rate, since companions are likely to exist over a large range of semimajor axes given that stellar companions do. Finally, achieving higher sensitivity (ours is nothing special) improves the yield per target by bringing older and lower mass companions into the observable region of parameter space.

Many thanks go to the MIRLIN team at the Jet Propulsion Laboratory. The operators of the Palomar 200 inch telescope provided their usual highly capable assistance in carrying out the observations. Observations at the Palomar Observatory were made as part of a continuing collaborative agreement between Palomar Observatory and the Jet Propulsion Laboratory. This work was performed in part at the Jet Propulsion Laboratory, which is operated by the California Institute of Technology under contract with the National Aeronautics and Space Administration.

REFERENCES

Boss, A. P. 1995, Science, 267, 360
Fischer, D. A., & Marcy, G. W. 1992, ApJ, 396, 178
Leggett, S. K. 1992, ApJS, 82, 351
Marcy, G. W., & Butler, R. P. 1998, in ASP Conf. Ser. 154, The Tenth Cambridge Workshop on Cool Stars, Stellar Systems, and the Sun, ed. R. A. Donahue & J. A. Bookbinder (San Francisco: ASP), in press
Mayor, M. 1998, in ASP Conf. Ser. 154, The Tenth Cambridge Workshop on Cool Stars, Stellar Systems, and the Sun, ed. R. A. Donahue & J. A. Bookbinder (San Francisco: ASP), in press
Nakajima, T., Oppenheimer, B. R., Kulkarni, S., Golimowski, D. A., Matthews, K., & Durrance, S. T. 1995, Nature, 378, 463
Nelson, J. A., Rappaport, S., & Joss, P. C. 1993, ApJ, 404, 723 (NRJ)
Pollack, J. B. 1984, ARA&A, 22, 389
Pollack, J. B., Hubickyj, O., Bodenheimer, P., Lissauer, J. J., Podalak, M., & Greenzweig, Y. 1996, Icarus, 124, 62
Ressler, M., Werner, M., Van Cleve, J., & Chou, H. A. 1994, Exp. Astron., 3, 277
Trilling, D. E., Benz, W., Guillot, T., Lunine, J. I., Hubbard, W. B., & Burrows, A. 1998, ApJ, 500, 428